

# Anomalous Resonance Frequency Shift of a Microelectromechanical Oscillator in Superfluid $^3\text{He-B}$

P. Zheng<sup>1</sup>  · W. G. Jiang<sup>1</sup> · C. S. Barquist<sup>1</sup> · Y. Lee<sup>1</sup> · H. B. Chan<sup>2</sup>

Received: 21 December 2016 / Accepted: 2 February 2017 / Published online: 16 February 2017  
© Springer Science+Business Media New York 2017

**Abstract** A superfluid  $^3\text{He}$  film with a thickness of  $1.25\ \mu\text{m}$  was studied using a micro-electromechanical oscillator at various pressures of 9.2, 18.2, 25.2, and 28.6 bars. The oscillator was driven in the linear damping regime where the damping coefficient is independent of the velocity of the oscillator. The resonance frequency shows weak temperature and pressure dependences in the low temperature limit. An inertia coefficient of  $\approx 0.1$  was obtained in the ballistic regime. When the temperature rose from the lowest temperature, the resonance frequency of the resonator exhibited an unusual behavior, a rapid increase beyond the intrinsic value as temperature increases, for 9.2 and 18.2 bars.

**Keywords** Quantum fluids · Superfluid  $^3\text{He}$  film · MEMS oscillators

## 1 Introduction

A generic nature of unconventional pairing, which is responsible for many exotic properties in unconventional superconductors and superfluids, is that the scattering off boundaries or impurities leads to pair breaking [1,2]. This property has been used as a main criterion for unconventional pairing in superconducting materials through disorder/impurity-dependent suppression of the transition temperature. Superfluid  $^3\text{He}$

---

✉ P. Zheng  
pzheng@ufl.edu

Y. Lee  
yoonslee@phys.ufl.edu

<sup>1</sup> Department of Physics, University of Florida, Gainesville, FL 32611-8440, USA

<sup>2</sup> Department of Physics, The Hong Kong University of Science and Technology, Clear Water Bay, Kowloon, Hong Kong

is a prime model system for studying the unconventional nature of Cooper pairs, owing to its clearly identified p-wave pairing and well-understood properties of the bulk fluid. Near boundaries, the components of the order parameter are selectively suppressed by surface scattering, depending on the boundary conditions [3–6]. As a consequence, midgap bound states, called the surface Andreev bound states (SABS), are spatially localized near the surface within the coherence length,  $\xi_0 = \hbar v_F / 2\pi k_B T_c$ , where  $\hbar$  is the Planck's constant,  $v_F$  is the Fermi velocity,  $k_B$  is the Boltzmann constant, and  $T_c$  is the transition temperature of bulk superfluid. Therefore, confinement of superfluid  $^3\text{He}$  into a geometry with at least one dimension comparable to the coherence length makes prominent the influence of the boundary effects on the thermodynamic and transport properties of the superfluid [7–9]. The detection of SABS in superfluid  $^3\text{He}$  is difficult as a result of the lack of an appropriate probe for the uncharged fluid. Nevertheless, various works have suggested the existence of SABS [10–18].

Among many types of confinement, a slab geometry with a thickness of  $D$  comparable to the coherence length is widely considered for studying the size effect on superfluid  $^3\text{He}$ . The phase diagram for superfluid  $^3\text{He}$  film is theoretically found drastically different from that for bulk fluid, with both  $T_c$  and the temperature of the A–B phase transition suppressed [8, 19–22]. For films of a few coherence lengths thick, the region of the A phase in the phase diagram extends to lower temperatures and pressures because the surface-induced order parameter distortion favors the A phase over the distorted B phase [9, 21]. The competition between the surface and bulk sets a critical thickness, below which the A phase (or the planar phase, which is degenerate with the A phase in the weak coupling limit) is stable down to  $T = 0$  [21, 22]. Furthermore, it is also predicted that at an even smaller critical thickness superfluidity disappears in films [8, 23, 24]. Recently, the stripe phase that breaks translational symmetry in superfluid  $^3\text{He}$  is predicted to emerge between the B phase and the A (planar) phase in the phase diagram of the reduced temperature and the reduced thickness,  $D/\xi_0$  [25]. This phase is predicted to be robust for a wide range of temperatures, pressures, and boundary conditions [26, 27].

Early experiments investigating the effects of slab confinement show that the superfluid transition temperature, superfluid density, and critical current are all suppressed as the film thickness decreases. In these experiments, films are formed in a stack of polymer membranes separated by tiny spacer spheres with a specific diameter on the order of microns [28, 29], or on a highly polished metal surfaces at the saturated vapor pressure [30–33]. Techniques such as nuclear magnetic resonance [28, 29], torsion pendulum [29, 31], and third sound spectrum [33] are used for identifying the pairing state or determining the superfluid density. Flow of superfluid film is driven by either electrostatic forces [30] or level difference between reservoirs [32] for measuring its flow rate and identifying the superfluid transition temperature.

An apparent drawback of previous methods of forming films is the difficulty of creating films with uniform and well-defined thickness. With the advanced nanolithography technology, new methods have been developed for creating superfluid  $^3\text{He}$  films to overcome the difficulty. The superfluid  $^3\text{He}$  film is either confined in nanofluidic cavities [34–36] or balanced by interdigitated electrodes [37, 38]. The thickness of the films is well defined via either the nanofabrication process of the cavity or the calibrated control of the electrostatic driving force applied by the interdigitated electrodes [39].

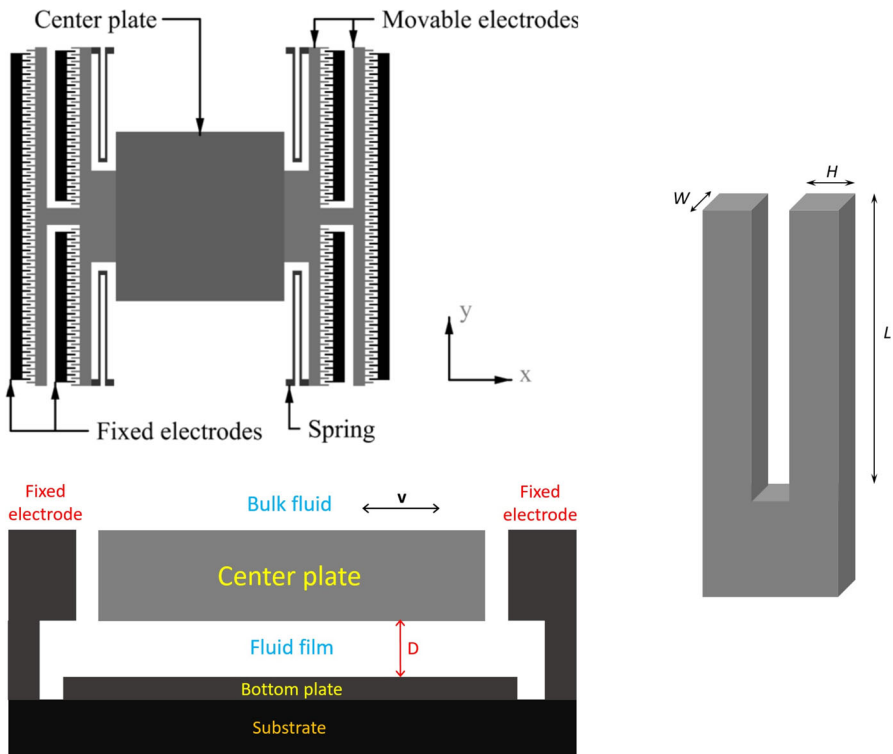


**Fig. 1** (Color figure online) Schematics of a typical MEMS device and a TF. (Left top) Top view of the MEMS device. The *light-colored regions* are movable parts, and the *dark-colored regions* are anchored to the substrate [48]. (Left bottom) Side view of the MEMS device. The *horizontal arrow* represents the direction of the oscillation of the shear mode [50]. (Right) Schematic of a TF where  $L$  is the length of prongs,  $H$  is the thickness of a prong, and  $W$  is the width of a prong. The values of these quantities of the two TFs are listed in Table 1

A SQUID-based NMR technique was developed for high sensitivity measurements on the single film formed in the nanofluidic chamber [40]. The mechanical resonance of torsion pendulums was used for measuring the superfluid density in the film [36].

Besides torsion pendulums [36,41], various resonators immersed in liquid  $^3\text{He}$ , such as vibrating wires [42,43], tuning forks [44,45], moving wires [14], and nanoelectromechanical devices [46], have been successfully implemented to investigate the properties of bulk normal and superfluid  $^3\text{He}$ . We have developed a resonator, based on microelectromechanical (MEMS) technology [47,48], to study liquid  $^3\text{He}$  films in both the normal phase [49] and the B phase [50,51]. The MEMS devices are fabricated to have a movable plate which can be electrostatically driven to oscillate in its own plane (called the shear mode). The plate is suspended above the substrate by four serpentine springs, maintaining a uniform gap of 0.75, 1.25, or  $2.0\ \mu\text{m}$  (Fig. 1). A fluid film is formed in the gap when such a device is immersed in the sample. The properties of the film may be inferred from the resonance features of the MEMS

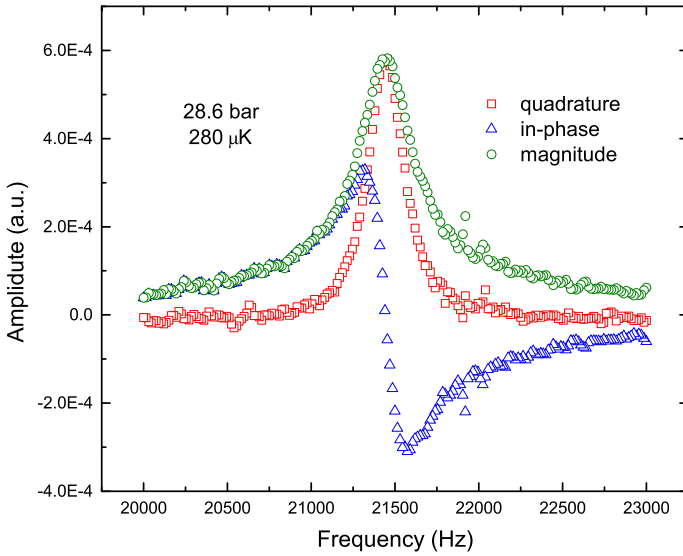


**Fig. 2** (Color figure online) Resonance spectrum of the device in superfluid  $^3\text{He}$  measured at 28.6 bar and 280  $\mu\text{K}$ . The magnitude channel of the spectrum is fitted to the Lorentzian model to extract the full width at half maximum (FWHM) and the resonance frequency

devices. In this paper, we report the unexpected frequency shift of the resonance in the ballistic regime of the B phase.

## 2 Experiment

The MEMS device used in this measurement has a mobile plate with 2  $\mu\text{m}$  thickness and 200  $\mu\text{m}$  lateral size. The gap,  $D$ , of the device is 1.25  $\mu\text{m}$  (see Fig. 1). The atomic force microscopy study of the MEMS surfaces shows that the average height variation of the polysilicon surface is  $\approx 10$  nm, while their lateral cluster size is  $\approx 150$  nm [47]. Therefore, the surface of the plate and substrate is diffusive since these length scales are much larger than the Fermi wavelength of the  $^3\text{He}$  quasiparticles. The shear mode of the device was studied with a symmetric capacitance bridge circuit [52]. Figure 2 demonstrates the resonance spectra of the device in superfluid  $^3\text{He}$  at 28.6 bar and 280  $\mu\text{K}$ . Resonance features such as full width at half maximum (FWHM) and resonance frequency were extracted from the resonance spectra by fitting them to the Lorentzian. The details of the MEMS devices and the measurement scheme have been reported elsewhere [47, 52, 53].

Two quartz tuning forks (TFs) were immersed in the same superfluid about 5 mm above the MEMS device: one was provided by the Lancaster Low Temperature group (called the *Lan* TF), and the other was a commercial Citizen TF (called the *Cit* TF). Their resonance spectra were measured simultaneously with those of the MEMS device during the experiment. Figure 1 shows a schematic of a TF with prongs of length  $L$ , thickness  $H$ , and width  $W$ , whose values for both TFs are listed in Table 1.

**Table 1** List of parameters of the tuning forks used in the experiments. The dimension symbols are illustrated in Fig. 1

Type	$L$	$H$	$W$	$f_0$	$\gamma$	$Q$
Lancaster	3100	90	75	8563.41	0.0173	$4.9 \times 10^5$
Citizen	3200	410	260	32702.35	0.135	$2.4 \times 10^5$

The units of the dimensions are in  $\mu\text{m}$ . The resonance frequency  $f_0$  and the FWHM  $\gamma$  (in Hz) are the intrinsic values measured in vacuum at 4 K. Quality factor  $Q$  is calculated as  $f_0/\gamma$

The MEMS device was cooled in liquid  $^3\text{He}$  to a base temperature of about  $250 \mu\text{K}$  at pressures of 9.2, 18.2, 25.2, and 28.6 bars. The resonance spectra were acquired upon warming from the base temperature with a typical warming rate of  $30 \mu\text{K/h}$ . The PLTS-2000 [54] was adopted as the temperature scale above 0.9 mK, below which the Florida scale [55] was used. The FWHM of the *Lan* TF was calibrated to determine the temperature below 0.6 mK [44, 45], above which a  $^3\text{He}$  melting curve thermometer was used. A magnetic field of 14 mT for a Pt NMR thermometer was applied to the superfluid in the direction perpendicular to the plane of the film except for one of the 28.6 bar measurements. For 28.6 bar, a measurement of resonators in superfluid in zero magnetic field was also performed. No significant difference was observed.

### 3 Results and Discussion

The resonance features of the MEMS and the TFs were measured at 4 K in vacuum. The residual gas in the cell was so rarefied that the measured FWHM and the resonance frequency could be regarded as the intrinsic properties of the resonators at the low temperatures. The resonance frequencies are 21545.08 Hz for the MEMS, 8563.41 Hz for the *Lan* TF, and 32702.35 Hz for the *Cit* TF. The quality factors are  $3.0 \times 10^5$ ,  $4.9 \times 10^5$ , and  $2.4 \times 10^5$ , respectively. These intrinsic quantities are determined solely by the material and geometry of the resonators. The spring constants of the serpentine springs, which can be calculated from the intrinsic resonance frequency and the bare mass of the resonators, are assumed to be unchanged below 4 K.

When liquid  $^3\text{He}$  is condensed in the cell below 1 K, the resonance features of the resonators change immediately. The resonance peak broadens as a result of the additional damping exerted by the fluid on the resonators. Meanwhile, the resonance frequency,  $f_0$ , decreases due to the mass enhancement of the resonators that is caused by the coupling of the surrounding fluid. For a fluid with a density of  $\rho$ , there are two significant contributions to the mass enhancement  $\delta m$  [44]:

$$\delta m = C_m \rho V + C_\delta \rho S \delta, \tag{1}$$

where the first term characterizes the mass of the potential flow around the resonators by which a volume of  $C_m V$  of the fluid is displaced. Here,  $C_m$  is the inertia coefficient representing the ratio of the volume of the displaced fluid to that of the oscillating object,  $V$ . The second term represents the drag force experienced by the object that is

90° phase shifted from the velocity. It can also be understood as the fluid clamped to the surface of the resonator with a characteristic thickness of the penetration depth  $\delta$ , which can be expressed as

$$\delta = \sqrt{\frac{2\eta}{\rho\omega}}, \quad (2)$$

where  $\eta$  is the viscosity of the fluid and  $\omega$  is the angular frequency of the oscillation.  $C_\delta$  is the coefficient measuring the volume of the clamped fluid in terms of the quantity  $S\delta$ , where  $S$  is the total surface area of the object.

When the liquid  $^3\text{He}$  becomes a superfluid at  $T_c$ , the mean free path of the quasiparticles continues to increase as the temperature decreases. The superfluid-resonator system enters the ballistic regime when the mean free path becomes larger than the characteristic size of the resonator. The interaction between the superfluid and the resonators can be modeled by ballistic scatterings of the quasiparticles off the resonators. Due to the isotropic energy gap in the energy spectrum of the quasiparticles, the damping of the resonators in the fluid drops exponentially with temperature and approaches the intrinsic value at the base temperature [43]. In addition, no fluid is clamped to the oscillator in the ballistic regime. The only contribution to the mass enhancement reduces to the displacement of the fluid [the first term in Eq. (1)], which is mainly determined by the geometry of the resonator [43].

Figures 3 and 4 show the resonance frequency shifts,  $\delta f_0$ , and the FWHM,  $\gamma$ , of the TFs and MEMS against the reduced temperature in  $^3\text{He-B}$  for each pressure. Below  $0.3 T_c$ , the FWHM of the *Lan* TF decreases rapidly and approaches the intrinsic value (0.0173 Hz) at the lowest temperature. The FWHM is actually used as thermometry in the ballistic regime and therefore strictly follows Boltzmann temperature dependence in Fig. 3. The damping of the MEMS, on the other hand, is four orders of magnitude higher than the intrinsic value (0.071 Hz) even at  $0.1 T_c$ . The anomalously high damping of the MEMS in the superfluid in the low temperature limit is ascribed to the presence of the surface states at the interface of the superfluid and the plate [50].

The frequency shifts are acquired by subtracting the corresponding intrinsic value from the measured resonance frequencies. The frequency shift of the two TFs saturates below  $0.3 T_c$ , which is a result of the temperature-independent displacement of the fluid. Pressure dependence of the saturation value can be clearly seen for both TFs. In this very range the FWHM keeps increasing since the density of the quasiparticles increases with temperature. When the temperature increases above  $0.3 T_c$ , the resonance frequency starts to decrease further due to the fluid clamped to the resonator. All observations obey the expectation mentioned above.

However, the temperature and pressure dependences of the resonance frequency shift of the MEMS are characteristically different from those of the TFs (Fig. 4). In the ballistic regime where the resonance frequency saturates against temperature, the frequency shift of the MEMS displays much weaker pressure dependence than that of the TFs. A frequency shift of  $\approx 85$  Hz is found in the low temperature limit. The resonance frequency of an oscillator is inversely proportional to the square root of

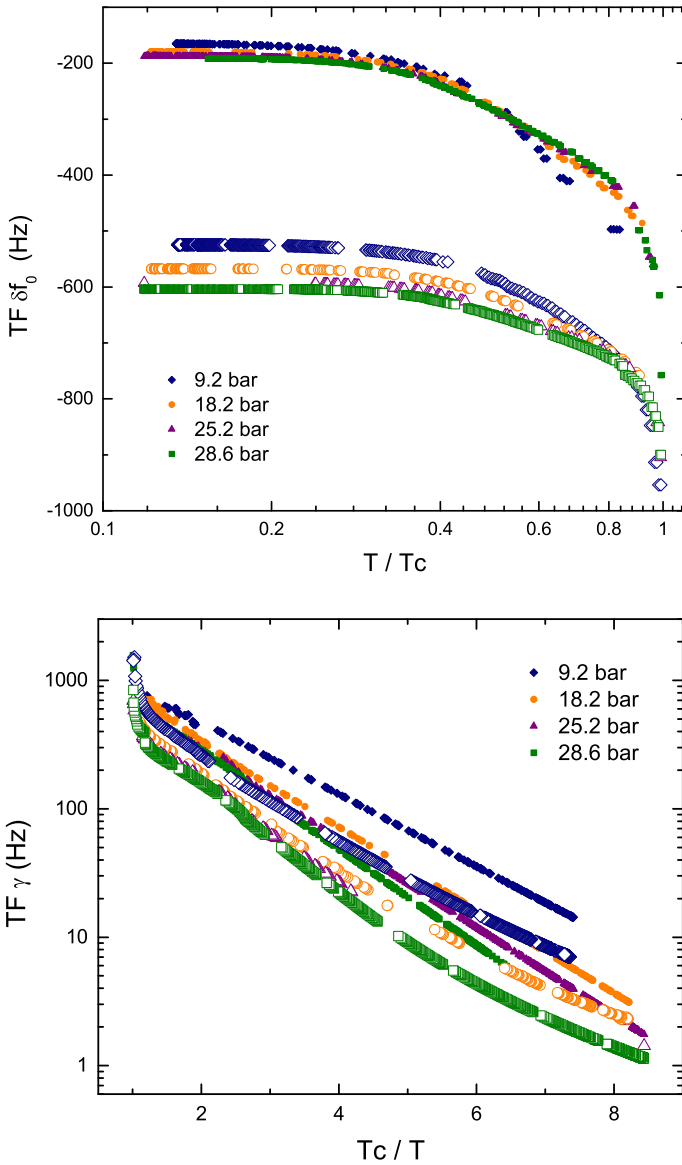


**Fig. 3** (Color figure online) Resonance frequency shift (*top*) and the FWHM (*bottom*) of the TFs against the reduced temperature at various pressures. The *solid symbols* represent the data of the *Lan* TF, while the *empty symbols* represent those of the *Cit* TF. Temperature reading is actually determined by the FWHM of the *Lan* TF using the Boltzmann dependence, leading to a strict linear behavior of the data in an Arrhenius scale. The FWHM of the *Cit* TF deviates from the linear behavior in the low temperature limit, which is probably because the FWHM approaches the intrinsic value (0.135 Hz). In the low temperature limit, the resonance frequency approaches saturation values, showing the ballistic behavior of the quasiparticles in the superfluid

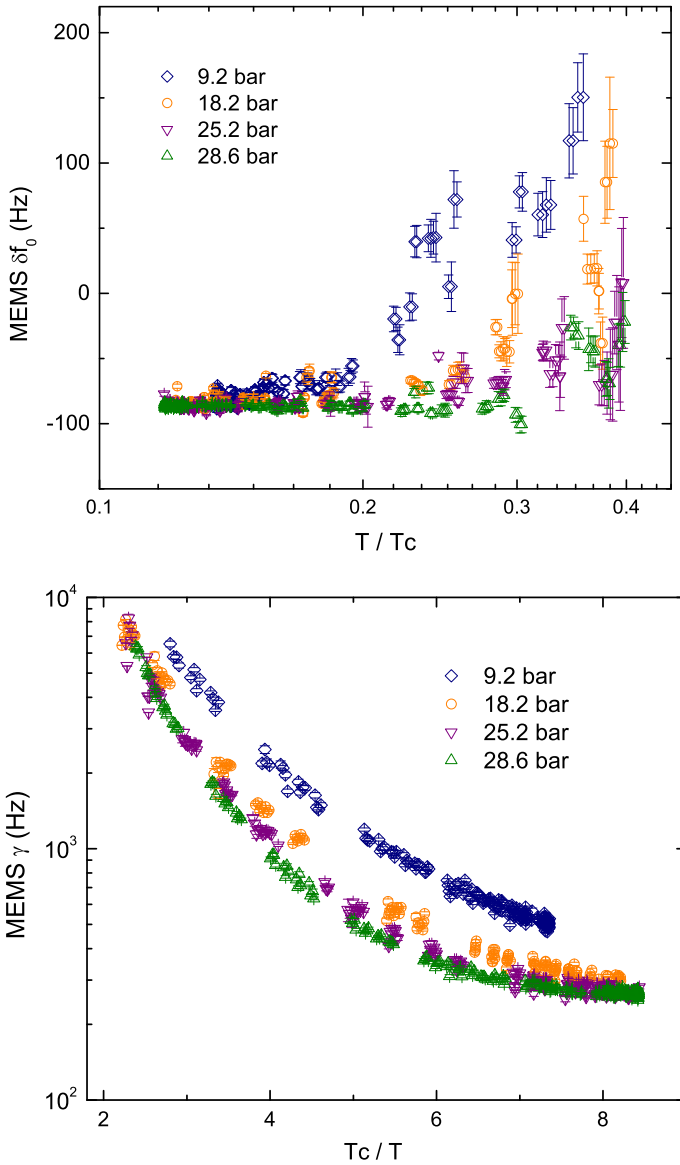


**Fig. 4** (Color figure online) Resonance frequency shift (*top*) and the FWHM (*bottom*) of the MEMS against the reduced temperature at various pressures. In the low temperature limit, an additional damping deviates the data from linear behavior in the Arrhenius scale [50], while the resonance frequency reaches saturation values. As the temperature increases, the frequency of the MEMS increases for 9.2 and 18.2 bar, which is contradictory to the expectation based solely on the mass loading effect. The *error bars* come from the standard deviation of the four consecutive measurements of the resonance curve in the same condition. As the temperatures increases, the signal-to-noise ratio decreases as a result of the increasing damping, which makes difficult the Lorentzian fitting



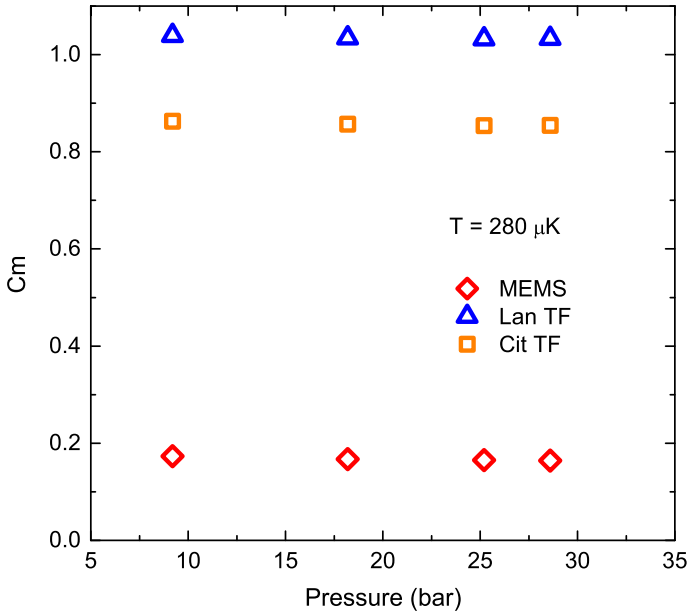


**Fig. 5** (Color figure online) Inertia coefficient  $C_m$  against the pressure for both MEMS and TFs. The inertia coefficient is almost independent of pressure. Its value is 0.17, 1.03, and 0.86 for the MEMS, the *Lan* TF, and the *Cit* TF, respectively

its effective mass. Therefore, the decrease in the resonance frequency  $\delta f_0$  is directly related to the additional loading mass  $\delta m$  due to the displacement of the fluid:

$$\frac{\delta f_0}{f_0} = -\frac{1}{2} \frac{\delta m}{m} = -\frac{1}{2} \frac{\rho}{\rho_{Si}} C_m, \tag{3}$$

where  $m$  is the intrinsic effective mass of the oscillator in vacuum and  $\rho_{Si}$  is the density of the material of the oscillating object. The inertia coefficients,  $C_m$ , of the MEMS and both TFs can be evaluated based on the density of the fluid and the frequency shift. Figure 5 shows the inertia coefficients of both the MEMS and the TFs for each pressure. The inertia coefficients of all three resonators show little pressure dependence, which justifies that the coefficient depends only on the geometry of the resonator. The plate of the MEMS has a large aspect ratio of lateral length to thickness ( $\approx 100:1$ ). Therefore, the volume of the fluid displaced by the narrow front and rear edges of the plate is much less than the volume of the plate, and the inertia coefficient should be much less than 1. On the other hand, the inertia coefficient of the TFs is expected to be close to 1, since the aspect ratio of the prongs is on the order of unity [45]. Equation (3) shows that the pressure dependence of the frequency shift stems only from that of the fluid density. Therefore, the frequency shift of the MEMS has a much weaker pressure dependence than that of the TFs as a result of its much lower inertia coefficient.

Another remarkable difference between resonance features of the MEMS and the TFs is that when the temperature increases to  $0.2 T_c$  for 9.2 bar and  $0.3 T_c$  for 18.2 bar,

the resonance frequency of the MEMS starts to increase from the saturation value in the low temperature limit. The maximum resonance frequency is even larger (by about 150 Hz) than the intrinsic value measured at 4 K. This anomalous increase in resonance frequency at 9.2 and 18.2 bar can also be seen clearly in the plot of the frequency shift against the FWHM (Fig. 6). For the other two higher pressures, the resonance frequency does not increase at FWHM of  $\approx 1500$  Hz. Since the mass of the resonator can never be less than its bare value, the simultaneous increase in both the FWHM and the resonance frequency may suggest the increase in the effective spring constant of the serpentine springs. It is unlikely that this value varies significantly over such a narrow temperature window in the submillikelvin region due to material properties of polysilicon. However, if there is some emergent restoring mechanism coupled to the resonator, the resonance frequency may increase without the change of the total mass of the resonator.

We do not believe this anomalous positive frequency shift is related to trapped vortex lines, which may cause extra stiffness. Our study of a MEMS device in superfluid  $^4\text{He}$  (He II) showed that vortex lines could be trapped in the gap due to the unique geometry of the MEMS.<sup>1</sup> The MEMS device in He II showed strong hysteresis persisting for an extended period of time when turbulence was generated by a nearby tuning fork. However, these vortex lines could be removed by driving the MEMS with high driving forces or warming the sample to the normal state and then cool back down. In the experiment in  $^3\text{He-B}$ , multiple independent cooldowns produced consistent spectra at a given temperature and pressure [50]. Furthermore, during each thermal cycle, the MEMS was regularly driven with high driving force to the nonlinear regime, where a substantial number of quasiparticles were generated [51]. Severe heating due to the quasiparticle generation should be able to alter the structure of the trapped vortex lines. But the spectrum recovered to the shape right before the heating after a reasonable relaxation time, which is inconsistent with the presence of trapped vortex lines.

Vorontsov and Sauls predicted an inhomogeneous superfluid phase, a stripe phase in superfluid  $^3\text{He}$  films with a domain structure of alternating degenerate B phases [25]. Wiman and Sauls found that the stripe phase is also stable at higher pressures and various boundary conditions [26]. The rough surfaces may be able to pin the domain walls since the thickness of the domain walls is of the order of the coherence length  $\xi_0$  [26], which is comparable to the surface roughness of the MEMS [47]. The distortion of the domain wall may provide an additional restoring force for the oscillator, leading to the increase in the frequency at 9.2 and 18.2 bar. It appears that the onset temperature for the rise of resonance frequency increases with pressure. Therefore, it is possible that for 25.2 and 28.6 bars the onset temperature may be so high that the large damping in the superfluid prevents the MEMS from generating a well-defined Lorentzian peak.

The strong coupling Ginzburg–Landau calculation shows the phase transition between the B phase and the stripe phase occurs when the thickness of the film is around  $12\xi_0$  for  $T \approx 0.6T_c$  [26]. For our device, the reduced thickness of the film is 65 at 28.6 bar and 35 at 9.2 bar, where the predicted temperature window of the stripe phases in the phase diagram is almost zero. However, recent measurements on

---

<sup>1</sup> To be published elsewhere.

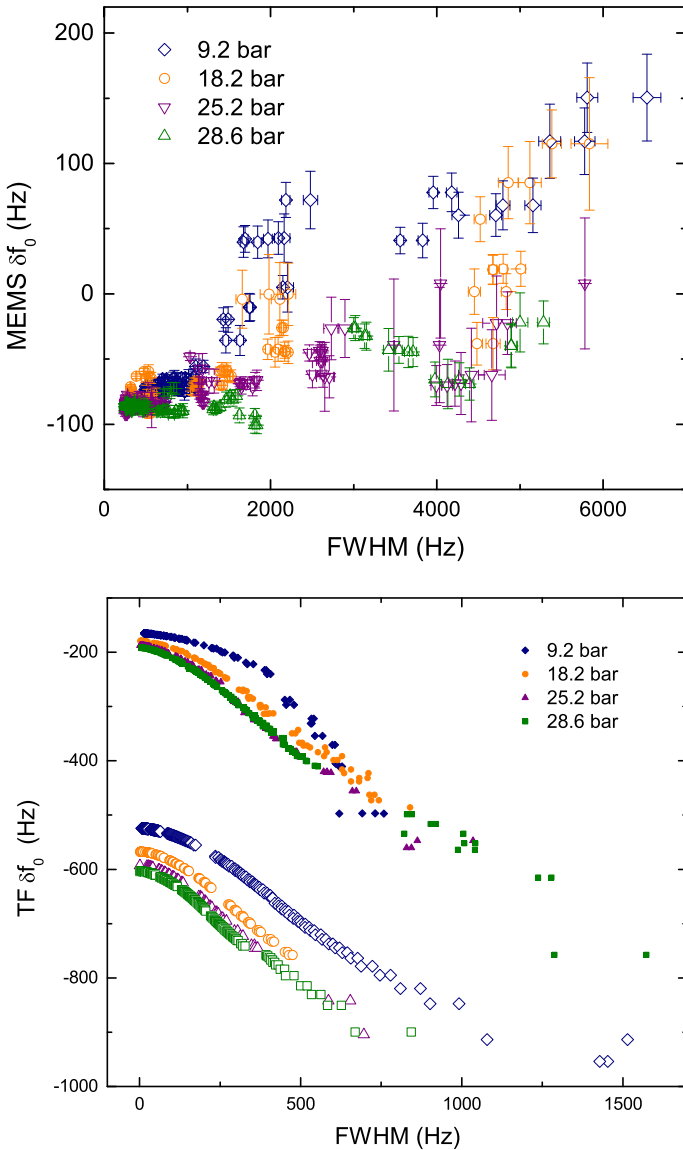


**Fig. 6** (Color figure online) Resonance frequency shift of the MEMS (*top*) and TFs (*bottom*) against the corresponding FWHM. In the TF plot, *solid symbols* represent the data of the *Lan* TF, while *empty symbols* represent those of the *Cir* TF. The anomalous increase in the resonance frequency for 9.2 and 18.2 bar is not seen for 25.2 and 28.6 bar at similar value of the quality factor

superfluid  $^3\text{He}$  confined in slab cavity of reduced thickness,  $D/\xi_\Delta = 10\text{--}14$ , did not yield evidence of the stripe phase [34,36]. The coherence length  $\xi_\Delta(T)$  is defined as  $\hbar v_F / (\sqrt{10} \Delta(T))$  and varies with temperature.

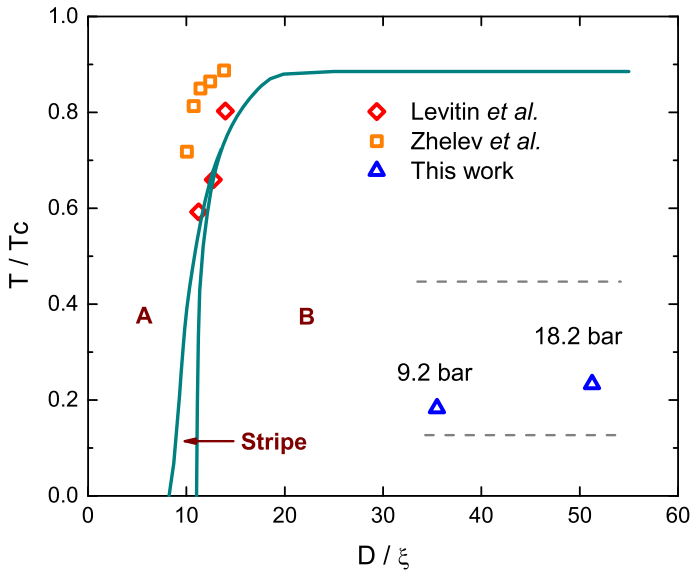


**Fig. 7** (Color figure online) Experimental parameters for various measurements in the temperature-confinement plane. The confinement is represented by the reduced gap,  $D/\xi$ , where the temperature-dependent coherence length is defined as  $\hbar v_F / (\sqrt{10}\Delta(T))$  [34]. Also plotted is the stripe phase boundaries for a diffusive boundary at 3 bar obtained using a strong coupling Ginzburg–Landau theory [26] (solid lines). The associated coherence length is  $\xi_0$  as defined in the beginning of the paper. For our measurement, the reduced temperatures at which the resonance frequency of the MEMS starts to increase are shown for 9.2 and 18.2 bar (triangles). The gray horizontal dashed lines indicate the temperature range of measurements for each pressure. Also plotted are the results from previous measurements on superfluid films confined in nanofluidic chambers using NMR [34] (diamonds) and torsion pendulum [36] (squares)

Figure 7 shows the experimental parameters (reduced temperature vs reduced thickness) of the measurements done by Levitin et al. [34] and Zhelev et al. [36], in addition to this work. Also plotted is the calculated stripe phase boundaries for a diffusive boundary at 3 bar obtained using a strong coupling Ginzburg–Landau theory [26]. Levitin et al. measured the A–B phase transition of a superfluid film confined in a slab cavity with a thickness of  $0.7 \mu\text{m}$  [34]. The data shown are for the onset temperature of the A–B transition on warming for diffusive boundaries at various pressures. No evidence associated with the stripe phase is found using the SQUID-based NMR. Zhelev et al. measured the A–B phase transition using a torsion pendulum for a film confined in a nanofluidic cavity with a thickness of  $1.08 \mu\text{m}$  [36]. The data shown are for the onset temperature of the A–B transition on warming for specular boundaries at various pressures. The A phase is observed in the parametric space where the stripe phase is predicted, although they suggest that small supercooling observed in the film may be caused by a new B phase nucleation mechanism mediated by the stripe phase. The failure of detecting the stripe phase at the predicted region may suggest the consideration of influence of other aspects on the phase diagram such as the dispersion relation of the surface bound states and the interaction between the bound states from the boundaries in close proximity.

To clarify whether the peculiar increase in the frequency shift comes from the presence of the film, we have developed MEMS devices with the substrate etched away. The moving plate in direct contact with the bulk fluid on both sides would help us identify the influence of the superfluid film on the resonance feature. We also plan to preplate the MEMS with  $^4\text{He}$  to alter the boundary condition of the film [29, 56–59] since the stability of the stripe phase is also influenced by the boundary condition. Furthermore, we also designed MEMS devices with greater mass of the plate so that well-defined Lorentzian could be acquired at even higher temperatures.

## 4 Conclusions

A MEMS device with a gap of  $1.25\ \mu\text{m}$  was studied in superfluid  $^3\text{He}$ . Its resonance frequency shift at the low temperature limit implies a coefficient of inertia of  $\approx 0.1$ , much smaller than that of the TFs submerged in the same fluid. The anomalous increase in resonance frequency of the MEMS oscillator at 9.2 and 18.2 bars suggests an additional restoring mechanism of unknown origin at this point.

**Acknowledgements** We would like to acknowledge the Lancaster Low Temperature group for providing quartz tuning forks as one of the TF thermometers. This work is supported by the National Science Foundation, Grant No. DMR-1205891 (YL).

## References

1. A.A. Abrikosov, L.P. Gor'kov, Sov. Phys. JETP **12**, 1243 (1961)
2. L.J. Buchholtz, G. Zwirknagl, Phys. Rev. B **23**, 5788 (1981). doi:[10.1103/PhysRevB.23.5788](https://doi.org/10.1103/PhysRevB.23.5788)
3. V. Ambegaokar, P.G. de Gennes, D. Rainer, Phys. Rev. A **9**, 2676 (1974). doi:[10.1103/PhysRevA.9.2676](https://doi.org/10.1103/PhysRevA.9.2676)
4. W. Zhang, J. Kurkijärvi, E.V. Thuneberg, Phys. Rev. B **36**, 1987 (1987). doi:[10.1103/PhysRevB.36.1987](https://doi.org/10.1103/PhysRevB.36.1987)
5. Y. Nagato, M. Yamamoto, K. Nagai, J. Low Temp. Phys. **110**, 1135 (1998). doi:[10.1023/A:1022368301143](https://doi.org/10.1023/A:1022368301143)
6. A.B. Vorontsov, J.A. Sauls, Phys. Rev. B **68**, 064508 (2003). doi:[10.1103/PhysRevB.68.064508](https://doi.org/10.1103/PhysRevB.68.064508)
7. G. Barton, M.A. Moore, J. Low Temp. Phys. **21**, 489 (1975). doi:[10.1007/BF01141605](https://doi.org/10.1007/BF01141605)
8. L.H. Kjøldman, J. Kurkijärvi, D. Rainer, J. Low Temp. Phys. **33**, 577 (1978). doi:[10.1007/BF00115576](https://doi.org/10.1007/BF00115576)
9. A.L. Fetter, S. Ullah, J. Low Temp. Phys. **70**, 515 (1988). doi:[10.1007/BF00682163](https://doi.org/10.1007/BF00682163)
10. Y. Aoki, Y. Wada, M. Saitoh, R. Nomura, Y. Okuda, Y. Nagato, M. Yamamoto, S. Higashitani, K. Nagai, Phys. Rev. Lett. **95**, 075301 (2005). doi:[10.1103/PhysRevLett.95.075301](https://doi.org/10.1103/PhysRevLett.95.075301)
11. K. Nagai, Y. Nagato, M. Yamamoto, S. Higashitani, J. Phys. Soc. Jpn. **77**, 111003 (2008). doi:[10.1143/JPSJ.77.111003](https://doi.org/10.1143/JPSJ.77.111003)
12. S. Murakawa, Y. Tamura, Y. Wada, M. Wasai, M. Saitoh, Y. Aoki, R. Nomura, Y. Okuda, Y. Nagato, M. Yamamoto, S. Higashitani, K. Nagai, Phys. Rev. Lett. **103**, 155301 (2009). doi:[10.1103/PhysRevLett.103.155301](https://doi.org/10.1103/PhysRevLett.103.155301)
13. H. Choi, J.P. Davis, J. Pollanen, W.P. Halperin, Phys. Rev. Lett. **96**, 125301 (2006). doi:[10.1103/PhysRevLett.96.125301](https://doi.org/10.1103/PhysRevLett.96.125301)
14. D.I. Bradley, S.N. Fisher, A.M. Guénault, R.P. Haley, C.R. Lawson, G.R. Pickett, R. Schanen, M. Skyba, V. Tsepelin, D.E. Zmееv, Nat. Phys. **12**, 1017 (2016). doi:[10.1038/nphys3813](https://doi.org/10.1038/nphys3813)
15. C.A.M. Castelijns, K.F. Coates, A.M. Guénault, S.G. Mussett, G.R. Pickett, Phys. Rev. Lett. **56**, 69 (1986). doi:[10.1103/PhysRevLett.56.69](https://doi.org/10.1103/PhysRevLett.56.69)
16. G.E. Volovik, JETP Lett. **90**, 398 (2009). doi:[10.1134/S0021364009170172](https://doi.org/10.1134/S0021364009170172)
17. J.P. Davis, J. Pollanen, H. Choi, J.A. Sauls, W.P. Halperin, A.B. Vorontsov, Phys. Rev. Lett. **101**, 085301 (2008). doi:[10.1103/PhysRevLett.101.085301](https://doi.org/10.1103/PhysRevLett.101.085301)

18. J. Elbs, C. Winkelmann, Y.M. Bunkov, E. Collin, H. Godfrin, *J. Low Temp. Phys.* **148**, 749 (2007). doi:[10.1007/s10909-007-9428-4](https://doi.org/10.1007/s10909-007-9428-4)
19. Y. Kuroda, A.D.S. Nagi, *Phys. B* **85**, 131 (1977). doi:[10.1016/0378-4363\(76\)90105-4](https://doi.org/10.1016/0378-4363(76)90105-4)
20. T. Fujita, M. Nakahara, *Prog. Theor. Phys.* **64**, 396 (1980). doi:[10.1143/PTP.64.396](https://doi.org/10.1143/PTP.64.396)
21. Y.H. Li, T.L. Ho, *Phys. Rev. B* **38**, 2362 (1988). doi:[10.1103/PhysRevB.38.2362](https://doi.org/10.1103/PhysRevB.38.2362)
22. Y. Nagato, K. Nagai, *Phys. B* **284–288**, 269 (2000). doi:[10.1016/S0921-4526\(99\)02594-6](https://doi.org/10.1016/S0921-4526(99)02594-6)
23. Z. Tešanović, O.T.V. and, *Phys. Rev. B* **34**, 7610 (1986). doi:[10.1103/PhysRevB.34.7610](https://doi.org/10.1103/PhysRevB.34.7610)
24. J. Hara, K. Nagai, *Prog. Theor. Phys.* **76**, 1237 (1986). doi:[10.1143/PTP.76.1237](https://doi.org/10.1143/PTP.76.1237)
25. A.B. Vorontsov, J.A. Sauls, *Phys. Rev. Lett.* **98**, 045301 (2007). doi:[10.1103/PhysRevLett.98.045301](https://doi.org/10.1103/PhysRevLett.98.045301)
26. J.J. Wiman, J.A. Sauls, *J. Low Temp. Phys.* **184**, 1054 (2016). doi:[10.1007/s10909-016-1632-7](https://doi.org/10.1007/s10909-016-1632-7)
27. K. Aoyama, *J. Phys. Soc. Jpn.* **85**, 094604 (2016). doi:[10.7566/JPSJ.85.094604](https://doi.org/10.7566/JPSJ.85.094604)
28. A.I. Ahonen, M. Krusius, M.A. Paalanen, *J. Low Temp. Phys.* **25**, 421 (1976). doi:[10.1007/BF00655840](https://doi.org/10.1007/BF00655840)
29. M.R. Freeman, R.S. Germain, E.V. Thuneberg, R.C. Richardson, *Phys. Rev. Lett.* **60**, 596 (1988). doi:[10.1103/PhysRevLett.60.596](https://doi.org/10.1103/PhysRevLett.60.596)
30. J.C. Davis, A. Amar, J.P. Pekola, R.E. Packard, *Phys. Rev. Lett.* **60**, 302 (1988). doi:[10.1103/PhysRevLett.60.302](https://doi.org/10.1103/PhysRevLett.60.302)
31. J. Xu, B.C. Crooker, *Phys. Rev. Lett.* **65**, 3005 (1990). doi:[10.1103/PhysRevLett.65.3005](https://doi.org/10.1103/PhysRevLett.65.3005)
32. S.C. Steel, J.P. Harrison, P. Zawadzki, A. Sachrajda, *J. Low Temp. Phys.* **95**, 759 (1994). doi:[10.1007/BF00754714](https://doi.org/10.1007/BF00754714)
33. A.M.R. Schechter, R.W. Simmonds, R.E. Packard, J.C. Davis, *Nature* **396**, 554 (1998). doi:[10.1038/25090](https://doi.org/10.1038/25090)
34. L.V. Levitin, R.G. Bennett, A. Casey, B. Cowan, J. Saunders, D. Drung, T. Schurig, J.M. Parpia, *Science* **340**, 841 (2013). doi:[10.1126/science.1233621](https://doi.org/10.1126/science.1233621)
35. L.V. Levitin, R.G. Bennett, E.V. Surovtsev, J.M. Parpia, B. Cowan, A.J. Casey, J. Saunders, *Phys. Rev. Lett.* **111**, 235304 (2013). doi:[10.1103/PhysRevLett.111.235304](https://doi.org/10.1103/PhysRevLett.111.235304)
36. N. Zhelev, T.S. Abhilash, E.N. Smith, R.G. Bennett, X. Rojas, L.V. Levitin, J. Saunders, J.M. Parpia, *ArXiv: 1610.07186* (2016)
37. M. Saitoh, H. Ikegami, H. Mukuda, K. Kono, *Phys. B* **329**, 131 (2003). doi:[10.1016/S0921-4526\(02\)01930-0](https://doi.org/10.1016/S0921-4526(02)01930-0)
38. M. Saitoh, H. Ikegami, K. Kono, *Phys. Rev. Lett.* **117**, 205302 (2016). doi:[10.1103/PhysRevLett.117.205302](https://doi.org/10.1103/PhysRevLett.117.205302)
39. M. Saitoh, H. Ikegami, H. Mukuda, K. Kono, *J. Low Temp. Phys.* **134**, 357 (2004). doi:[10.1023/B:JOLT.0000012579.18512.bc](https://doi.org/10.1023/B:JOLT.0000012579.18512.bc)
40. L.V. Levitin, R.G. Bennett, A. Casey, B. Cowan, J. Saunders, D. Drung, T. Schurig, J.M. Parpia, B. Ilic, N. Zhelev, *J. Low Temp. Phys.* **175**, 667 (2014). doi:[10.1007/s10909-014-1145-1](https://doi.org/10.1007/s10909-014-1145-1)
41. A. Casey, J. Parpia, R. Schanen, B. Cowan, J. Saunders, *Phys. Rev. Lett.* **92**, 255301 (2004). doi:[10.1103/PhysRevLett.92.255301](https://doi.org/10.1103/PhysRevLett.92.255301)
42. D.C. Carless, H.E. Hall, J.R. Hook, *J. Low Temp. Phys.* **50**, 583 (1983). doi:[10.1007/BF00683497](https://doi.org/10.1007/BF00683497)
43. A.M. Guénault, V. Keith, C.J. Kennedy, S.G. Mussett, G.R. Pickett, *J. Low Temp. Phys.* **62**, 511 (1986). doi:[10.1007/BF00683408](https://doi.org/10.1007/BF00683408)
44. R. Blaauwgeers, M. Blažková, M. Človečko, V.B. Eltsov, R. de Graaf, J. Hosio, M. Krusius, D. Schmoranzler, W. Schoepe, L. Skrbek, P. Skyba, R.E. Solntsev, D.E. Zmeev, *J. Low Temp. Phys.* **146**, 537 (2007). doi:[10.1007/s10909-006-9279-4](https://doi.org/10.1007/s10909-006-9279-4)
45. D.I. Bradley, P. Crookston, S.N. Fisher, A. Ganshin, A.M. Guénault, R.P. Haley, M.J. Jackson, G.R. Pickett, R. Schanen, V. Tsepelin, *J. Low Temp. Phys.* **157**, 476 (2009). doi:[10.1007/s10909-009-9982-z](https://doi.org/10.1007/s10909-009-9982-z)
46. M. Defoort, S. Dufresnes, S.L. Ahlstrom, D.I. Bradley, R.P. Haley, A.M. Guénault, E.A. Guise, G.R. Pickett, M. Poole, A.J. Woods, V. Tsepelin, S.N. Fisher, H. Godfrin, E. Collin, *J. Low Temp. Phys.* **183**, 284 (2016). doi:[10.1007/s10909-015-1392-9](https://doi.org/10.1007/s10909-015-1392-9)
47. M. González, P. Zheng, E. Garcell, Y. Lee, H.B. Chan, *Rev. Sci. Instrum.* **84**, 025003 (2013). doi:[10.1063/1.4790196](https://doi.org/10.1063/1.4790196)
48. M. González, P. Bhupathi, B.H. Moon, P. Zheng, G. Ling, E. Garcell, H.B. Chan, Y. Lee, *J. Low Temp. Phys.* **162**, 661 (2011). doi:[10.1007/s10909-010-0247-7](https://doi.org/10.1007/s10909-010-0247-7)
49. M. González, W.G. Jiang, P. Zheng, C.S. Barquist, H.B. Chan, Y. Lee, *Phys. Rev. B* **94**, 014505 (2016). doi:[10.1103/PhysRevB.94.014505](https://doi.org/10.1103/PhysRevB.94.014505)
50. P. Zheng, W.G. Jiang, C.S. Barquist, Y. Lee, H.B. Chan, *Phys. Rev. Lett.* **117**, 195301 (2016). doi:[10.1103/PhysRevLett.117.195301](https://doi.org/10.1103/PhysRevLett.117.195301)

51. P. Zheng, W.G. Jiang, C.S. Barquist, Y. Lee, H.B. Chan, Phys. Rev. Lett. **118**, 065301 (2017)
52. P. Zheng, W.G. Jiang, C.S. Barquist, Y. Lee, H.B. Chan, J. Low Temp. Phys. **183**, 313 (2016). doi:[10.1007/s10909-015-1388-5](https://doi.org/10.1007/s10909-015-1388-5)
53. C.S. Barquist, J. Bauer, T. Edmonds, P. Zheng, W.G. Jiang, M. González, Y. Lee, H.B. Chan, J. Phys.: Conf. Ser. **568**, 032003 (2014). doi:[10.1088/1742-6596/568/3/032003](https://doi.org/10.1088/1742-6596/568/3/032003)
54. R.L. Rusby, M. Durieux, A.L. Reesink, R.P. Hudson, G. Schuster, M. Kühne, W.E. Fogle, R.J. Soulen, E.D. Adams, J. Low Temp. Phys. **126**, 633 (2002). doi:[10.1023/A:1013791823354](https://doi.org/10.1023/A:1013791823354)
55. W. Ni, J.S. Xia, E.D. Adams, P.S. Haskins, J.E. McKisson, J. Low Temp. Phys. **101**, 305 (1995). doi:[10.1007/BF00754593](https://doi.org/10.1007/BF00754593)
56. S.M. Tholen, J.M. Parpia, Phys. Rev. Lett. **68**, 2810 (1992). doi:[10.1103/PhysRevLett.68.2810](https://doi.org/10.1103/PhysRevLett.68.2810)
57. D. Kim, M. Nakagawa, O. Ishikawa, T. Hata, T. Kodama, H. Kojima, Phys. Rev. Lett. **71**, 1581 (1993). doi:[10.1103/PhysRevLett.71.1581](https://doi.org/10.1103/PhysRevLett.71.1581)
58. Y. Wada, S. Murakawa, Y. Tamura, M. Saitoh, Y. Aoki, R. Nomura, Y. Okuda, Phys. Rev. B **78**, 214516 (2008). doi:[10.1103/PhysRevB.78.214516](https://doi.org/10.1103/PhysRevB.78.214516)
59. S. Murakawa, M. Wasai, K. Akiyama, Y. Wada, Y. Tamura, R. Nomura, Y. Okuda, Phys. Rev. Lett. **108**, 025302 (2012). doi:[10.1103/PhysRevLett.108.025302](https://doi.org/10.1103/PhysRevLett.108.025302)